

# Supplemental Material: High thermal conductivity and thermal boundary conductance of homoepitaxially grown gallium nitride (GaN) thin films

*Yee Rui Koh, Md Shafkat Bin Hoque, Habib Ahmad, David H. Olson, Zeyu Liu, Jingjing Shi, Yekan Wang, Kenny Huynh, Eric R. Hoglund, Kiumars Aryana, James M. Howe, Mark S. Goorsky, Samuel Graham, Tengfei Luo, Jennifer K. Hite, W. Alan Doolittle, and Patrick E. Hopkins*

Yee Rui Koh, Md Shafkat Bin Hoque, Kiumars Aryana  
Department of Mechanical and Aerospace Engineering, University of Virginia, Charlottesville, Virginia 22904, USA

David H. Olson  
Department of Mechanical and Aerospace Engineering, University of Virginia, Charlottesville, Virginia 22904, USA  
Present address: Laser Thermal Analysis, Inc., Charlottesville, Virginia 22902, USA

Habib Ahmad  
School of Electrical and Computer Engineering, Georgia Institute of Technology, Atlanta, Georgia, 30332, USA

Zeyu Liu, Tengfei Luo  
Department of Aerospace and Mechanical Engineering, University of Notre Dame, Notre Dame, Indiana 46556, USA

Jingjing Shi  
George W. Woodruff School of Mechanical Engineering, Georgia Institute of Technology, Atlanta, Georgia 30332, USA

Yekan Wang, Kenny Huynh, Mark S. Goorsky  
Department of Materials Science and Engineering, University of California, Los Angeles, California 90095, USA

Eric R. Hoglund, James M. Howe  
Department of Materials Science and Engineering, University of Virginia, Charlottesville, Virginia 22904, USA

Samuel Graham  
George W. Woodruff School of Mechanical Engineering, Georgia Institute of Technology, Atlanta, Georgia 30332, USA  
School of Materials Science and Engineering, Georgia Institute of Technology, Atlanta, Georgia 30332, USA

Jennifer K. Hite  
U.S. Naval Research Laboratory, Washington, D.C. 20375, USA

W. Alan Doolittle  
School of Electrical and Computer Engineering, Georgia Institute of Technology, Atlanta, GA, 30332, USA  
Email: alan.doolittle@ece.gatech.edu

Patrick E. Hopkins  
Department of Mechanical and Aerospace Engineering, University of Virginia, Charlottesville, Virginia 22904, USA  
Department of Materials Science and Engineering, University of Virginia, Charlottesville, Virginia 22904, USA  
Department of Physics, University of Virginia, Charlottesville, Virginia 22904, USA  
Email: phopkins@virginia.edu

\* Yee Rui Koh, Md Shafkat Bin Hoque, and Habib Ahmad contributed equally to this work

## S1. Cleaning procedure and Al deposition technique of the MBE-grown GaN thin films

Prior to the thin film growth, two-inch diameter HVPE semi-insulating GaN on sapphire wafers are chemically cleaned and back side metallized with 2  $\mu\text{m}$  of tantalum for uniform heating during growth. The metallized wafers are diced into 1 cm  $\times$  1 cm templates. The templates are solvent cleaned followed by a piranha (3 to 1 volume ratio of  $\text{H}_2\text{SO}_4$  to  $\text{H}_2\text{O}_2$ ) clean at 150  $^\circ\text{C}$  for 10 minutes and subsequently cleaned by 1:10 volume ratio of hydrofluoric acid to deionized water for 30 seconds to remove oxides from the templates' surface. The HVPE GaN templates are then outgassed for thermal cleaning at 200  $^\circ\text{C}$  for 20 minutes in an introductory chamber with a base pressure of  $\sim 1 \times 10^{-9}$  Torr followed by outgassing at 675  $^\circ\text{C}$  for 10 minutes in the growth chamber with a base pressure of  $\sim 1 \times 10^{-10}$  Torr. Ga-flashing is employed in order to achieve systematic improvement in the regrowth interface cleaning by three cycles of Ga-adsorption and Ga-desorption, at 600 and 710  $^\circ\text{C}$ , respectively.<sup>1</sup> The UID GaN films are grown at a substrate temperature of 650  $^\circ\text{C}$  and a III/V ratio of 1.8 followed by Al deposition at 200  $^\circ\text{C}$ . Similarly, the Mg-doped GaN films are grown at a substrate temperature of 600  $^\circ\text{C}$  and a III/V ratio of 1.5 followed by Al deposition at 200  $^\circ\text{C}$ . III/V ratios are measured *in situ* during growth by reflection high energy electron diffraction (RHEED) transients.

## S2. First-principles lattice dynamics (FPLD) calculations of pristine GaN

In these first-principles calculations, three different scattering mechanisms are included: the three-phonon scattering, the isotopic scattering, and the boundary scattering. An iterative process is used to get the converged phonon distribution and thermal conductivity using *ShengBTE*.<sup>2</sup> For the three-phonon scattering, a  $4 \times 4 \times 4$  q grid is used in the density functional perturbation theory<sup>3</sup> scheme to calculate the harmonic force constants using *Quantum Espresso*.<sup>4</sup> The third order force constants are calculated from a  $4 \times 4 \times 4$  supercell with eighth nearest neighbor cutoff via a finite difference method. The isotopic scattering is calculated based on the natural isotopic distribution of Ga and N. The boundary scattering, on the other hand, is considered by introducing an extra scattering term with  $v/L$ , where  $v$  is the magnitude of the phonon group velocity and  $L$  is the thickness of the calculation setup. This boundary scattering term assumes the GaN/GaN interface to be completely diffusive, i.e., all the phonons are scattered after travelling the  $L$  thickness.

### S3. TDTR measurements of GaN thin films

TDTR is an optical pump-probe technique that is widely used to characterize the thermal properties of bulk and thin film materials. In our TDTR setup, a Ti:Sapphire pulsed laser (central wavelength of 800 nm and repetition rate of 80 MHz) is split into a high-power pump and a low-power probe beam. The pump beam is frequency doubled to 400 nm before it is modulated by an electro-optic modulator (EOM). This modulated pump beam generates a small temperature rise at the sample surface. The time-delayed probe beam monitors the transient thermal response by measuring the thermoreflectance change with a balanced photodetector and a lock-in amplifier. The reflected probe signals are processed by fitting the ratio of in-phase to out-of-phase signal from the lock-in amplifier to a heat diffusion model.<sup>5-7</sup> For the TDTR measurements of this study, we use a 10X objective with  $1/e^2$  pump and probe diameters of  $\sim 17$  and  $10 \mu\text{m}$ , respectively. Furthermore, due to the small thickness of the GaN thin films, a high modulation frequency of 8.8 MHz is used. This high pump modulation frequency is essential to increase sensitivity to GaN thin film thermal conductivity and Al/GaN thermal boundary conductance. The uncertainty associated with TDTR measurements incorporates the standard deviation of multiple measurements across different spots, uncertainty associated with the Al transducer thickness and thermal conductivity, and GaN heat capacity.

For interpreting the TDTR data, we assume that the epitaxial GaN/GaN thermal boundary conductance is  $1000 \text{ MW m}^{-2} \text{ K}^{-1}$ . The sensitivity analysis for the 800 nm MBE-grown GaN film corresponding to this boundary conductance is presented in the Supplemental Material Figure S1(a). For comparison, we also include the sensitivity analysis corresponding to a GaN/GaN thermal boundary conductance of  $200 \text{ MW m}^{-2} \text{ K}^{-1}$ . Figure S1 (a) shows that despite the small thickness of the GaN film, TDTR measurements have adequate sensitivity to the GaN thin film thermal conductivity and Al/GaN thermal boundary conductance. It is also evident that when the GaN/GaN thermal boundary conductance is high (i.e.,  $1000 \text{ MW m}^{-2} \text{ K}^{-1}$ ), its influence on TDTR measurements is negligible. However, this influence becomes significant if the GaN/GaN boundary conductance is relatively lower (i.e.,  $200 \text{ MW m}^{-2} \text{ K}^{-1}$ ). Therefore, to check the accuracy of our high GaN/GaN thermal boundary conductance assumption, we measure the GaN

thin film thermal conductivity as a function of modulation frequency at different temperatures as presented in Figure S1(b). The sensitivity level of the GaN/GaN boundary conductance changes with modulation frequency. In addition, the GaN/GaN boundary conductance also varies with temperature.<sup>8-10</sup> Thus, the assumption of high GaN/GaN thermal boundary conductance can be considered valid if the obtained thin film thermal conductivity is consistent among different modulation frequencies at multiple temperatures. The measurements presented in Figure S1(b) show this consistency, thereby validating our assumption. Similar high thermal boundary conductances have also been reported in literature for other epitaxial interfaces.<sup>8,10-12</sup>

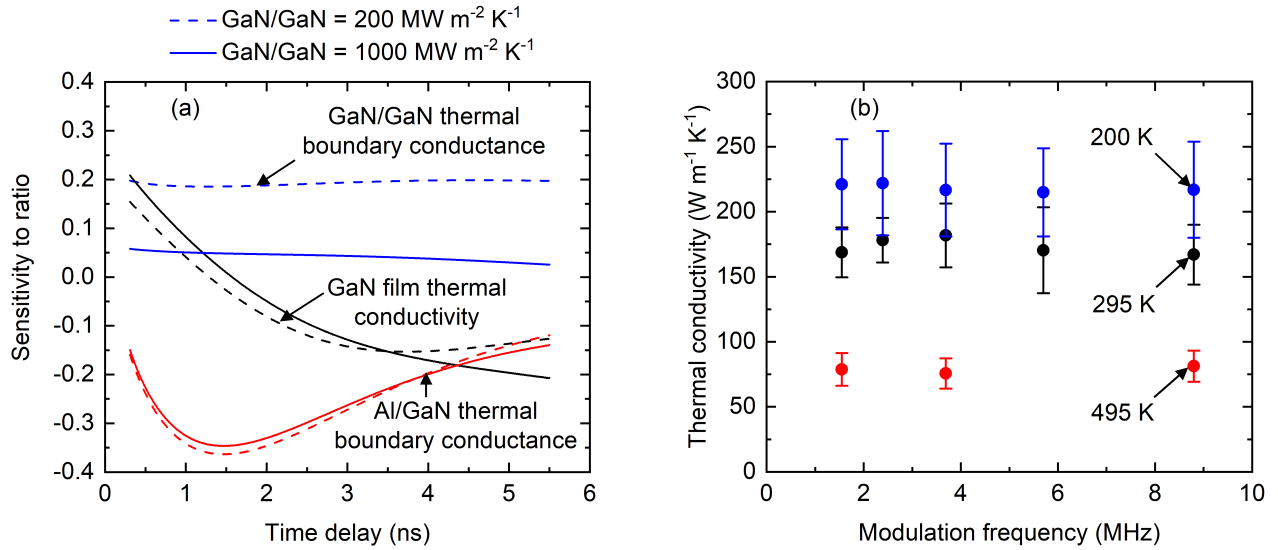


Figure S1: (a) Sensitivity analysis of TDTR measurements at 8.8 MHz modulation frequency for the 800 nm MBE-grown GaN film. The dashed and solid lines correspond to GaN/GaN thermal boundary conductances of 200 and 1000 MW m<sup>-2</sup> K<sup>-1</sup>, respectively. (b) Thermal conductivity of the 800 nm GaN film as a function of modulation frequency at 200, 295, and 495 K.

## S4. SSTR measurements of GaN thin films

In our SSTR setup, two continuous wave lasers of 532 and 786 nm wavelengths are used as the pump and probe beams, respectively. The pump is modulated at 100 Hz by a mechanical chopper before it is incident at the sample surface. At such low modulation frequency, the pump beam induces a steady-state temperature rise in the target sample. The probe beam then detects the temperature rise using a balanced photodetector and a lock-in amplifier. By varying the pump power, the incident heat flux at the sample surface and the resultant steady-state temperature rise are changed. By correlating the heat flux and temperature rise with Fourier’s law, the thermal conductivity of the sample is determined.<sup>13</sup>

In this study, we have selected three control samples for SSTR measurements: 1.9 and 2.1  $\mu\text{m}$  MOCVD-grown UID GaN thin films, and n-doped bulk HVPE GaN used as the substrate material. The thinner GaN films are excluded as measurements of thinner samples can be highly influenced by the GaN substrate or template properties. For these SSTR measurements, pump and probe beams of  $1/e^2$  radii of  $\sim 10 \mu\text{m}$  are co-axially focused onto the sample surface. The experimental proportionality constant,  $\gamma$ , is determined from a sapphire reference ( $35 \text{ W m}^{-1} \text{ K}^{-1}$ ) according to the procedure described in previous publications.<sup>14,15</sup>

The SSTR-measured thermal conductivities of the control samples are shown in Table S1. The SSTR uncertainty here accounts for the measurement repeatability, uncertainty in the  $\gamma$  value,<sup>13,14</sup> Al transducer thermal conductivity, and thermal boundary conductances. As evident in Table S1, SSTR measurements are in agreement with the TDTR-measured values. The SSTR measurements here represent the geometric mean of in-plane and cross-plane thermal conductivities, whereas the TDTR-measured values represent the cross-plane thermal conductivity.<sup>15</sup>

Table S1: Thermal conductivity of the control GaN samples measured by TDTR and SSTR

| Samples                   | Thermal conductivity<br>( $\text{W m}^{-1} \text{ K}^{-1}$ ) |              |
|---------------------------|--|--------------|
|                           | TDTR   | SSTR         |
| 1.9 $\mu\text{m}$ UID GaN | $196 \pm 20$   | $203 \pm 30$ |
| 2.1 $\mu\text{m}$ UID GaN | $195 \pm 20$   | $209 \pm 30$ |
| n-doped bulk HVPE GaN     | $210 \pm 17$   | $203 \pm 16$ |

## S5. Modal nonequilibrium Landauer method for calculating Al/GaN thermal boundary conductance

In this work, we use the modal non-equilibrium Landauer approach to calculate the thermal boundary conductance across the Al/GaN interface. Detailed descriptions of this method have been provided in Shi *et al.*<sup>16</sup> and Koh *et al.*<sup>10</sup> The phonon transmission coefficient at the Al/GaN interface is calculated with the diffuse mismatch model (DMM). The local non-equilibrium effect at the interface is considered with local temperature correction from the modal non-equilibrium Landauer method. The phonon properties (e.g., phonon density of states, group velocity) of GaN and Al are obtained from the density functional theory (DFT) calculations performed with VASP (Vienna Ab initio Simulation Package).

## References

- [1] Ahmad, H.; Anderson, T. J.; Gallagher, J. C.; Clinton, E. A.; Engel, Z.; Matthews, C. M.; Alan Doolittle, W. Beryllium doped semi-insulating GaN without surface accumulation for homoepitaxial high power devices. *Journal of Applied Physics* **2020**, *127*, 215703.
- [2] Li, W.; Carrete, J.; Katcho, N. A.; Mingo, N. ShengBTE: A solver of the Boltzmann transport equation for phonons. *Computer Physics Communications* **2014**, *185*, 1747–1758.
- [3] Baroni, S.; De Gironcoli, S.; Dal Corso, A.; Giannozzi, P. Phonons and related crystal properties from density-functional perturbation theory. *Reviews of modern Physics* **2001**, *73*, 515.
- [4] Giannozzi, P.; Baroni, S.; Bonini, N.; Calandra, M.; Car, R.; Cavazzoni, C.; Ceresoli, D.; Chiarotti, G. L.; Cococcioni, M.; Dabo, I., et al. QUANTUM ESPRESSO: a modular and open-source software project for quantum simulations of materials. *Journal of physics: Condensed matter* **2009**, *21*, 395502.
- [5] Cahill, D. G. Analysis of heat flow in layered structures for time-domain thermoreflectance. *Review of scientific instruments* **2004**, *75*, 5119–5122.
- [6] Schmidt, A. J.; Chen, X.; Chen, G. Pulse accumulation, radial heat conduction, and anisotropic thermal conductivity in pump-probe transient thermoreflectance. *Review of Scientific Instruments* **2008**, *79*, 114902.
- [7] Hopkins, P. E.; Serrano, J. R.; Phinney, L. M.; Kearney, S. P.; Grasser, T. W.; Harris, C. T. Criteria for cross-plane dominated thermal transport in multilayer thin film systems during modulated laser heating. *Journal of Heat Transfer* **2010**, *132*.
- [8] Costescu, R. M.; Wall, M. A.; Cahill, D. G. Thermal conductance of epitaxial interfaces. *Physical Review B* **2003**, *67*, 054302.
- [9] Donovan, B. F.; Szejewski, C. J.; Duda, J. C.; Cheaito, R.; Gaskins, J. T.; Peter Yang, C.-Y.; Constantin, C.; Jones, R. E.; Hopkins, P. E. Thermal boundary conductance across metal-gallium nitride interfaces from 80 to 450 K. *Applied Physics Letters* **2014**, *105*, 203502.

- [10] Koh, Y. R.; Shi, J.; Wang, B.; Hu, R.; Ahmad, H.; Kerdsonpanya, S.; Milosevic, E.; Doolittle, W. A.; Gall, D.; Tian, Z., et al. Thermal boundary conductance across epitaxial metal/sapphire interfaces. *Physical Review B* **2020**, *102*, 205304.
- [11] Koh, Y. K.; Cahill, D. G. Frequency dependence of the thermal conductivity of semiconductor alloys. *Physical Review B* **2007**, *76*, 075207.
- [12] Li, H.; Hanus, R.; Polanco, C. A.; Zeidler, A.; Koblmüller, G.; Koh, Y. K.; Lindsay, L. GaN thermal transport limited by the interplay of dislocations and size effects. *Physical Review B* **2020**, *102*, 014313.
- [13] Braun, J. L.; Olson, D. H.; Gaskins, J. T.; Hopkins, P. E. A steady-state thermoreflectance method to measure thermal conductivity. *Review of Scientific Instruments* **2019**, *90*, 024905.
- [14] Hoque, M. S. B.; Koh, Y. R.; Aryana, K.; Hoglund, E. R.; Braun, J. L.; Olson, D. H.; Gaskins, J. T.; Ahmad, H.; Elahi, M. M. M.; Hite, J. K.; Leseman, Z. C.; Doolittle, W. A.; Hopkins, P. E. Thermal conductivity measurements of sub-surface buried substrates by steady-state thermoreflectance. *Review of Scientific Instruments* **2021**, *92*, 064906.
- [15] Hoque, M. S. B.; Koh, Y. R.; Braun, J. L.; Mamun, A.; Liu, Z.; Huynh, K.; Liao, M. E.; Husain, K.; Cheng, Z.; Hoglund, E. R., et al. High In-Plane Thermal Conductivity of Aluminum Nitride Thin Films. *ACS Nano* **2021**, *15*, 9588–9599.
- [16] Shi, J.; Yang, X.; Fisher, T. S.; Ruan, X. Dramatic increase in the thermal boundary conductance and radiation limit from a nonequilibrium Landauer approach. *arXiv preprint arXiv:1812.07910* **2018**, 1–19.